Journal of Applied Physics

Effect of grain size on thin film stress and morphology using kinetic Monte Carlo simulations

Cite as: J. Appl. Phys. **128**, 145301 (2020); https://doi.org/10.1063/5.0023081
Submitted: 26 July 2020 . Accepted: 26 September 2020 . Published Online: 08 October 2020

Eric Chason, and Piyush Jagtap

Journal of Applied Physics ARTICLE scitation.org/journal/jap

Effect of grain size on thin film stress and morphology using kinetic Monte Carlo simulations

Cite as: J. Appl. Phys. **128**, 145301 (2020); doi: 10.1063/5.0023081
Submitted: 26 July 2020 · Accepted: 26 September 2020 ·
Published Online: 8 October 2020

Eric Chason[a] and Piyush Jagtap

AFFILIATIONS

School of Engineering, Brown University, Providence, Rhode Island 02912, USA

[a]**Author to whom correspondence should be addressed:** Eric_Chason@Brown.edu

ABSTRACT

A kinetic Monte Carlo simulation of polycrystalline thin film growth has been developed that enables the effects of stress to be included. The stress is modeled in terms of processes that happen at the grain boundary, i.e., the formation of new grain boundary lengths and diffusion of atoms from the surface. In this work, the simulation has been used to study the effect of grain size on the thin film stress and surface morphology evolution. Results are presented for different grain sizes, temperatures, and growth rates and the kinetics of relaxation when the growth is terminated. The results are interpreted in terms of rate equations developed to explain thin film stress evolution.

I. INTRODUCTION

Understanding the mechanisms controlling stress in thin films is motivated by the impact it can have on performance and reliability. Numerous studies have shown how the stress is modified by the processing conditions (growth rate[1–4] and temperature[2,5–11]) and microstructural evolution.[2,7,12,13] This suggests that the film growth kinetics can be used to control the resulting stress.

Multiple mechanisms have been proposed to explain the different aspects of thin film stress evolution during non-energetic deposition (e.g., thermal evaporation, electrodeposition). Useful discussions of the outstanding issues can be found in several reviews.[14–17] The formation of grain boundaries between adjacent grains has been proposed to lead to tensile stress[18–20] by reducing the interfacial energy. Diffusion of atoms from the surface into the grain boundary has been proposed as a mechanism to produce compressive stress.[21] A rate equation approach has been used to incorporate these mechanisms into an analytical model to predict the dependence of the stress on parameters such as the growth rate, atom mobility, grain size, and grain growth kinetics.[10]

The analytical model has been successfully applied to interpret experimental results for both non-energetic deposition[3,12,22,23] and, in an extended version, energetic deposition.[24,25] Kinetic parameters for the model have been determined by fitting it to data from experiments. It would be useful to develop a more fundamental understanding of these parameters so that the reasonableness of the fitting values can be evaluated. Moreover, this would allow the parameters to be predicted from other measurements besides stress or from calculations.

Additionally, it is difficult to capture the stochastic nature of film growth using rate equation approaches. The dynamics of adatom arrival, diffusion, cluster nucleation, and incorporation into the film are complex so that it is difficult to model parameters such as the concentration of mobile species on the surface. Understanding this would be useful because the surface supersaturation is proposed to be a driving force for compressive stress in the film.

An alternative modeling method for thin film growth that includes stochastic processes is the kinetic Monte Carlo (KMC) simulation.[26] In the KMC approach, the local environment around each mobile atom is monitored to determine the energetic barriers for motion in each possible direction. The surface evolution is simulated by allowing each atom to make transitions based on these transition rates. This approach has been very powerful in looking at the process of film growth and the evolution of thin film morphology.[26–28] Some have even used energetic particle deposition[29] to understand its impact on film evolution.

The generation of thin film stress is not typically considered in KMC because the strain fields are in the long range, whereas the diffusional events are governed by the local environment. In recent work, however, stress generation and relaxation have been incorporated into a KMC simulation by using the same approximations used in the rate equation model of film stress.[30] The stress is

assumed to be controlled by processes happening at the grain boundary and is assumed to be uniform across the grain, so that the impact of stress gradients on transport away from the grain boundary can be ignored.

In the initial report from this work,[30] the KMC model was used to study the flux of atoms into and out of the grain boundary along with the resulting evolution of the film stress. This work allowed the connection between the surface morphology, the rates of transitions between the surface and grain boundary, and the resulting stress to be studied as a function of temperature and growth rate. The results revealed the interplay between the supersaturation of mobile surface atoms that was created by the deposition flux and the corresponding rate at which atoms were incorporated into the grain boundary. At high deposition rates, the rate of atoms going into the grain boundary was found to have a power-law dependence on the deposition rate, which explains why the stress is more tensile for higher deposition rates.

To better understand how the conditions on the surface relate to the resulting stress, in the current work, the KMC approach is extended to explore the effect of grain size on thin film stress. This makes it possible to see how the surface morphology evolves in different regions near and far from the grain boundary for the same processing conditions. The resulting dependence of the steady-state stress on grain size, growth rate, and temperatures is interpreted in terms of different kinetic regimes that depend on the diffusion distance of deposited adatoms. For short diffusion distances, the conditions near the grain boundary are unaffected by conditions on the rest of the surface far from it. As the diffusion distance increases, the conditions near the grain boundary are affected by the surface farther from it. In addition, simulations of the relaxation/recovery kinetics when growth is interrupted/resumed explore how the stress is related to the rates of transitions into and out of the grain boundary under different conditions. These kinetics are also interpreted using a rate equation model that was developed to explain relaxation experiments.[31]

II. KINETIC MONTE CARLO SIMULATION AND STRESS MODEL

The results presented in this work are based on a kinetic Monte Carlo approach that has been described previously,[30,32,33] so it is only discussed briefly here. A schematic representation of some of the processes modeled by the simulation is shown in Fig. 1. The different colors correspond to heights that differ by one layer, and adatoms are represented by circles. The atoms move on a square lattice so that each atom can have up to four in-plane bonds and use a solid-on-solid model so that there are no empty sites below the surface.

The concept behind the simulation approach is that each atom can make transitions to neighboring sites based on the local morphology. The kinetics therefore depend on whether the atom has no neighbors (diffusion) or if it changes the number of in-plane bonds (attachment/detachment). Atoms can be added from the vapor (deposition) and can also make transitions into and out of a simulated grain boundary shown at one end of the simulation. This enables the development of stress to be considered and is discussed in detail below. The adjacent sides have periodic boundary

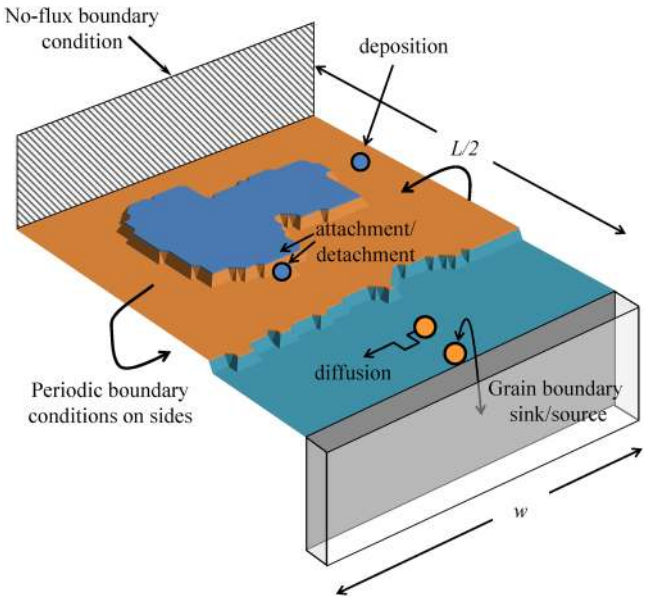

FIG. 1. Schematic of some of the kinetic processes modeled by the kinetic Monte Carlo simulation. The transitions shown correspond to adatom diffusion, attachment and detachment at step edges, and diffusion in and out of the grain boundary. The boundary conditions are indicated, i.e., periodic on both sides, no-flux at the top, and a grain boundary source/sink at the bottom. The energetics and rates associated with each type of transition are described in the text.

conditions. The side opposite to the grain boundary has a reflection (no-flux) boundary condition so that the simulated surface corresponds to half of a symmetric grain. The dimensions in each direction ($L/2$ and w) are shown at the sides of the model. The simulated surface size in the figure is 64×64, which corresponds to a grain size of $L = 128$. Other grain sizes of 256 and 512 are also considered in this work.

The transition rate from one surface site i to an adjacent site j is assumed to have an Arrhenius temperature dependence,

$$r(i,j) = \upsilon e^{\frac{-E(n_i,n_j)}{kT}}, \tag{1}$$

where $E(n_i, n_j)$ depends on the local morphology and υ is the attempt frequency. The activation barrier is different depending on whether the initial site corresponds to an isolated adatom (E_{adatom}), an atom attached to a step-edge (E_{edge}), or the one next to a vacancy ($E_{vacancy}$). In addition, if the diffusional jump corresponds to the breaking of in-plane bonds, an additional energy of $(n_i - n_j)E_{bond}$ is added to the diffusion barrier. The simulation keeps track of the transition rates at all atoms on the surface with fewer than four in-plane bands; if an atom has four nearest neighbors, it is assumed to be immobile. Individual atoms are then moved on the surface with a probability based on its transition rate relative to the total rate of all possible transitions.

KMC simulations do not typically consider the effect of stress since strain fields are in the long range while the transition rates

only depend on the local environment. To overcome this limitation, an approximation is used that was developed to explain stress in thin films.[16] In this picture, the stress is assumed to develop in the grain boundary during film growth and be uniform over the width of the grain.

To implement this, one edge of the simulation is made to act as a grain boundary. A tensile stress (σ_T) is assumed to be generated whenever two layers in adjacent grains grow together to form new segments of grain boundary, based on a mechanism proposed by Hoffman.[18] In addition, atoms are allowed to jump into or out of the boundary. Adding atoms into the boundary makes the stress more compressive/less tensile while removing atoms from the boundary has the opposite effect.

The resulting stress in the layer is then given by

$$\sigma = \sigma_T - N_{gb}\frac{M_f a^3}{L h_{gb} w}, \tag{2}$$

where a is the nominal size of the atom, L is the grain size, M_f is the biaxial modulus of the film, h_{gb} is the average height of the grain boundary, and w is the width of the simulation. Most importantly, N_{gb} is the net number of atoms that are incorporated into the grain boundary by jumps from the surface minus the number of atoms that have jumped out of the grain boundary. σ_T depends inversely on the square root of the grain size so that it can be expressed as $\sigma_{T,0}\left(\frac{L_{ref}}{L}\right)^{1/2}$, where $\sigma_{T,0}$ is the tensile stress when the grain size is equal to L_{ref}. This equation assumes that the diffusion of atoms within the grain boundary is high so that the stress is uniform throughout the thickness of the layer.

Atoms jumping into the grain boundary are the source of compressive stress in the film. The rate at which atoms jump into the grain boundary depends on the concentration of mobile surface atoms at its edge. This depends on the evolution of the surface morphology and is affected by the deposition rate as well as the nucleation of clusters and terraces on the surface that act as sinks for the atoms. Because it is the result of multiple stochastic kinetic processes, it is not possible to estimate this rate. In fact, understanding what determines the rate of atoms jumping into the grain boundary is one of the goals of developing these simulations. The relation between growth conditions, morphology evolution, and transition rates into the surface are considered in the discussion in Sec. IV.

Detailed balance requires that the possibility of atoms jumping out of the boundary must also be considered. The simulation assumes that there is an energetic barrier for diffusion from atoms at the top of the boundary onto the surface given by E_{eff}. Because the grain boundaries are assumed to be relatively stable, the value is chosen to be higher than for diffusion of adatoms. Stress in the film also changes the chemical potential of atoms in the grain boundary, which modifies the height of the barrier by σa^3. The total rate of atoms jumping out of the grain boundary is then given by

$$\left(\frac{dN_{gb}}{dt}\right)_{out} = \upsilon\left(\frac{w}{a}\right)X_{gb}e^{\frac{-(E_{eff}+\sigma a^3)}{kT}}, \tag{3}$$

where w/a is the number of sites at the top of the grain boundary and X_{gb} is the fraction of these sites that have mobile atoms.

III. SIMULATION RESULTS

The simulated surface is represented by a rectangular array with the height corresponding to the value of each array element. The surface is initially flat (all heights are zero) and then atoms are added to it at a rate determined by the deposition rate. The surface morphology evolves by either adding more atoms to the surface (from the vapor or the grain boundary) or allowing existing atoms to make transitions to neighboring sites according to the rates described in Eq. (1).

The boundary conditions are not the same at each edge of the surface. One edge corresponds to a grain boundary, which means that atoms can be removed from the surface by jumping into it or they can be added to the surface by jumping out of it. The rate for jumping into the grain boundary is described like any other surface transition rate [Eq. (1)] and depends on the configuration of neighbors around the atom at the edge of the grain. The rate of jumping out of the boundary depends on the stress in the layer as described in Eq. (3). The edge of the simulation opposite from the grain boundary has a reflection boundary condition so that the simulated surface corresponds to one half of a symmetric grain. The boundary conditions on the other two edges are periodic so that an atom that jumps off one side jumps onto the other side at the same point.

The simulations were performed over a range of processing conditions with growth rates that varied from 0.1 to 1 000 000 monolayers (ML)/s, temperatures of 300 and 400 K, and grain sizes of 128, 256, and 512 in units of the atomic size (a). The values of parameters used in the simulation are shown in Table I. These are the same values used in the previous simulations in Ref. 30. They do not correspond exactly to a particular material, but they are similar to what might be expected for Ni films.

Images of the surface morphology resulting from the simulation are shown in Fig. 2. Each image is made after 100 ML of deposition at a simulation temperature of (a) 300 K and (b) 400 K. The growth rate in each column has values of 10, 1000, and 100 000 monolayers/s from left to right (other growth rates were studied but their morphologies are not shown here). The grain size increases from the bottom ($L = 128$) to the top ($L = 512$) of each column. The horizontal and vertical scales are the same in all the images and the color of the surface is changed for each layer height. The lower right side of each image is the position of the grain boundary that can act as a sink or source. The upper left side of each simulation has a reflection boundary condition so each image corresponds to one half of a symmetric grain.

TABLE I. Values of parameters used in the simulation.

E_{adatom}	E_{edge}	$E_{vacancy}$	E_{bond}	E_{eff}	X_{gb}
0.25 eV	0.55 eV	2.0 eV	0.3 eV	0.85 eV	0.5
$\sigma_{T,0}$	M_f	υ	a	L_{ref}	w
1 GPa	300 GPa	10^{12}/s	0.3 nm	512 a	64 a

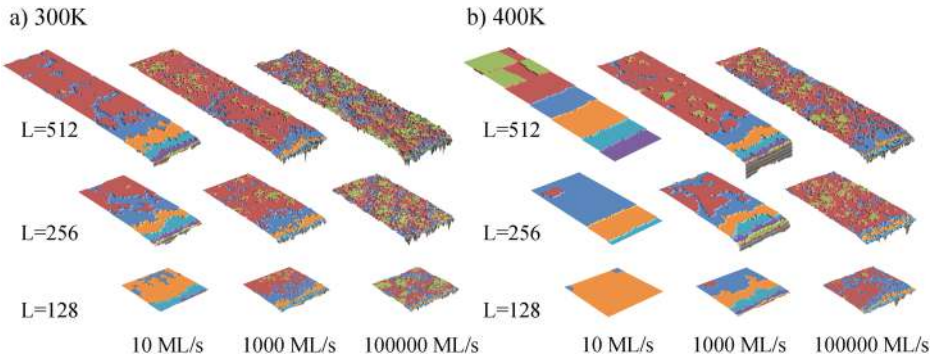

FIG. 2. Images of surface morphology after 100 monolayers of deposition at simulation temperatures of (a) 300 K and (b) 400 K. Grain size and growth rate are indicated in the figure.

The numbers of atoms going into and out of the grain boundary [$(N_{gb})_{in}$ and $(N_{gb})_{out}$] are kept track of by the simulation and used to calculate the stress. The evolution of these quantities with thickness depends on the growth rate and temperature; it has been discussed previously[30] so the time evolution is not shown here. The rate of each process reaches a steady-state value as the thickness increases. The net rate $[dN_{gb}/dt = (dN_{gb}/dt)_{in} - (dN_{gb}/dt)_{out}]$ at a steady-state is shown in Fig. 3 as a function of growth rate for different grain sizes at temperatures (a) 300 K and (b) 400 K. The near linearity of the data on a log–log plot suggests a power-law dependence on the growth rate, similar to what has been observed previously. The results for different grain sizes show that the power-law dependence remains almost the same if the size of the simulated grain is changed. A deviation with grain size is only observed at the lower growth rates studied.

The steady-state stress is shown in Fig. 4 as a function of growth rate and grain size. Results are shown for temperatures of (a) 300 K and (b) 400 K, and the grain size is indicated in the figure. Consistent with previous results, the stress changes from compressive at low growth rates to tensile at high growth rates. The transition between tensile and compressive stress depends on the deposition conditions and also on the grain size. For smaller grain sizes, the stress is more tensile at high growth rates and more compressive at low growth rates than for larger grain sizes. The growth rate for the transition from compressive to tensile is larger at the higher temperature for each grain size.

In addition to the steady-state stress, the kinetics of relaxation and recovery for different grain sizes were also studied. Figure 5 shows results for different grain sizes of (a) 512, (b) 256, and (c) 128. The growth was performed at a deposition rate of 10 monolayers/s and a temperature of 400 K. Initially, the growth flux is turned on until 20 monolayers are deposited. This is followed by a 32 s period where the growth flux is turned off and the film stress relaxes. After this, an additional 20 monolayers are deposited followed by another 32 s period of relaxation. The solid lines in the figure are the results of fitting the kinetics observed in the simulation to an analytical model.[31] Further details of this model are provided in Sec. IV.

IV. DISCUSSION

The goal of the following discussion is to relate the evolution of quantities monitored in the simulation to the underlying physical processes. Perceptions from these results are then applied to our understanding of thin film growth and stress evolution.

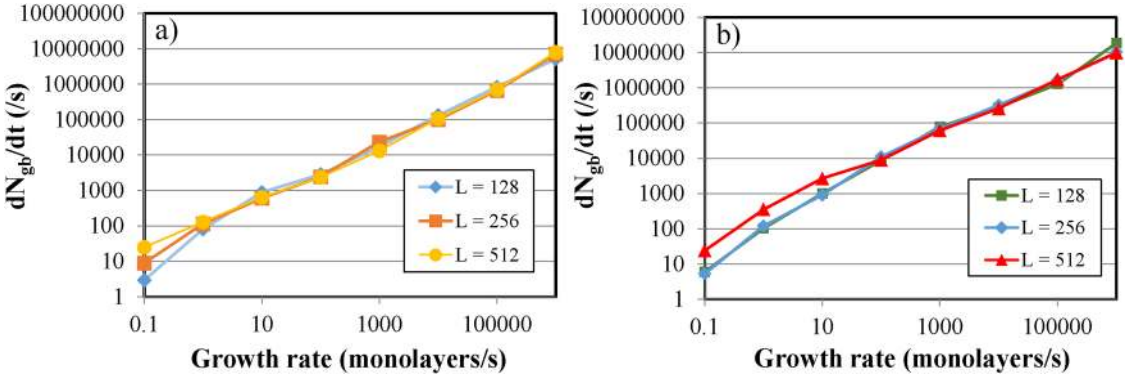

FIG. 3. Net transition rate (dN_{gb}/dt) of atoms jumping into and out of the grain boundary vs growth rate. Results are shown after 100 monolayers of deposition at simulation temperatures of (a) 300 K and (b) 400 K. Grain sizes are indicated in the figure.

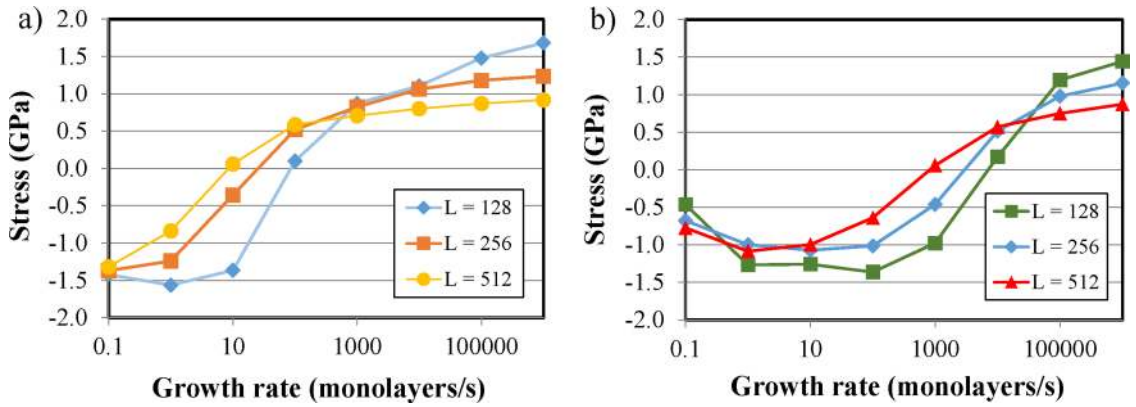

FIG. 4. Steady-state stress vs growth rate after 100 monolayers of deposition at simulation temperatures of (a) 300 K and (b) 400 K. Grain sizes are indicated in the figure.

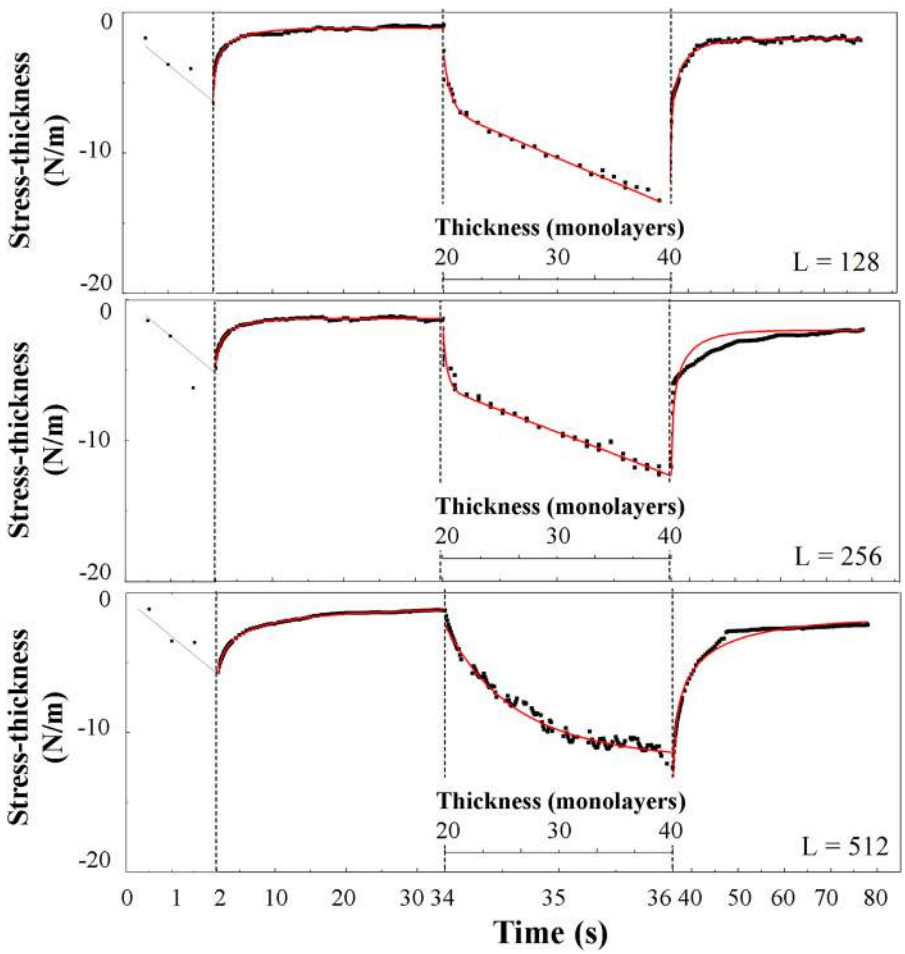

FIG. 5. Stress-thickness evolution for sequences of growth and relaxation at a temperature of 400 K. The deposition was performed at a growth rate of 10 monolayers/s. Grain size is indicated in the figure. The solid lines correspond to fitting the data to the models described in the text.

A. Surface morphology

The dependence of the surface morphology on simulation temperature and growth rate has been explored previously, but the current work extends this to study the effect of grain size as well. The dependence on the growth rate for each grain size can be seen by comparing the images across each row. The dependence on grain size at each growth rate can be seen by comparing images in the same column from top to bottom.

First, consider the growth at $T = 300$ K. At the highest growth rate and lowest temperature shown [$R = 100\,000$ ML/s, $T = 300$ K in Fig. 2(a)], the evolution is dominated by copious nucleation and growth of two-dimensional islands uniformly across the surface. In this regime, which we refer to as multilayer nucleation, the morphology is not strongly affected by the presence of the grain boundary. Therefore, the morphology is similar for the different grain sizes at this rate. This is consistent with the short diffusion distance of adatoms and correspondingly high concentration of adatoms on the surface during growth.

At the next lower growth rate shown ($R = 1000$ ML/s, $T = 300$ K), the presence of the grain boundary as a sink for atoms can be seen to affect the distribution of islands on the surface. Individual nuclei coalesce into terraces with edges that progress toward the grain boundary as the thickness increases. In this regime, referred to as 2D-nucleation and coalescence, step edges become apparent in the region of the surface near the grain boundary; the morphology away from the grain boundary shows more uniform nucleation of islands across it. As the steps approach the grain boundary, they pile up on each other as their motion across the surface slows down.

At a lower growth rate ($R = 10$ ML/s, $T = 300$ K, $L = 512$), most of the deposited atoms attach to existing steps and the morphology evolution is even more dominated by the propagation of well-organized step edges (step-flow growth). However, the morphology is somewhat different for this growth rate when the grain size is smaller ($L = 128$). In this case, a deposited adatom is likely to get to a sink (grain boundary or step-edge) before clustering with other adatoms, which keeps the surface concentration and island nucleation rates low (referred to as 2D-nucleation limited). The surface, therefore, remains quite flat and only a few steps sweep across the surface as it grows. Note that this occurs because new islands form by homogeneous nucleation so that the rate depends on concentration. In real systems, the presence of defects on the surface (e.g., screw dislocations) may be a source of new steps without the need for homogeneous nucleation.[34]

Similar results are seen in the simulations performed at 400 K [Fig. 2(b)]. However, the different types of behavior are moved to higher growth rates at this higher temperature. For instance, the steps are more well-organized for growth at 1000 ML/s at $T = 400$ K than they are at 300 K. This shows that the growth at 400 K occurs more deeply into the step-flow regime, indicating that the transition from 2D-nucleation to step-flow occurs at a higher growth rate. Similarly, the 2D-nucleation limited regime is more pronounced at $R = 10$ monolayers/s and $L = 128$ at 400 K than it is at 300 K.

Based on studies of stress in thin films,[16] a useful guide for thinking about this behavior is through the dimensionless parameter D/RL. Lowering the growth rate has a similar effect on the morphology evolution as raising the temperature. When D/RL is increased, the morphology evolution transitions from multilayer nucleation → 2D-nucleation and coalescence → step-flow → 2D-nucleation limited. The transitions between the types of evolution are not sharp, but the characteristic behavior can generally be identified in each regime.

The images of the surface suggest that R and T have a larger effect on the surface morphology than the grain size except for the highest values of D/RL. For low values of D/RL (e.g., $R = 100\,000$ ML/s, $T = 300$ K), the surface morphology appears to be similar for all three grain sizes. This is because the changes in morphology are localized near the grain boundary. As D/RL is increased, the effect of the grain boundary on the morphology spreads further into the surface away from the grain boundary. When the diffusion distance becomes comparable to the grain size, a transition to the 2D-nucleation limited behavior can be observed that occurs first for the smaller grain size.

B. Transition rates into and out of grain boundary

In the rate equation model for stress, the transition rates between the surface and grain boundary are important because they control the stress in the film.[16] The supersaturation on the surface created by the deposition flux is the driving force for compressive stress in the film. In return, the stress in the film also modifies the rate at which atoms jump out of the grain boundary [Eq. (3)].

The different types of surface morphology evolution discussed above affect the corresponding rate of atoms jumping from the surface into the grain boundary. The net rate of atoms jumping in and out of the grain boundary (Fig. 3) follows a power-law dependence on growth rate described by R^x. Averaged across the grain sizes, the exponent x has a value of 0.81 ± 0.04 and 0.84 ± 0.06 for temperatures of 300 and 400 K, respectively, with the rates for 400 K slightly higher than the rates for 300 K. The behavior does not depend strongly on the grain size, but a small deviation develops at lower growth rates with the larger grain size having a slightly higher net transition rate.

The weak dependence on the grain size is consistent with the fact that the surface morphology also does not depend strongly on the grain size. As seen in Fig. 2, the grain boundary only affects the surface morphology relatively close to it except for the lowest growth rate/highest temperature. Since the rates of atoms jumping from the surface into the grain boundary depend on the local morphology, this also controls the net transition rate. An increase in the concentration of adatoms in the middle of the grain does not immediately affect the rates into the grain boundary. Atoms deposited far from the grain boundary cannot diffuse to it without crossing many steps and are, therefore, likely to be incorporated into an existing step or nucleate a new island before reaching the grain boundary. The way that the region far from the boundary ultimately affects the stress evolution is through the propagation of steps from the middle of the grain to the boundary in step-flow mode.

The rate of atoms jumping into the grain boundary [$(dN_{gb}/dt)_{in}$] depends on the supersaturation on the surface, which is the driving force for compressive stress The behavior of $(dN_{gb}/dt)_{in}$ can be observed directly in the simulations by turning

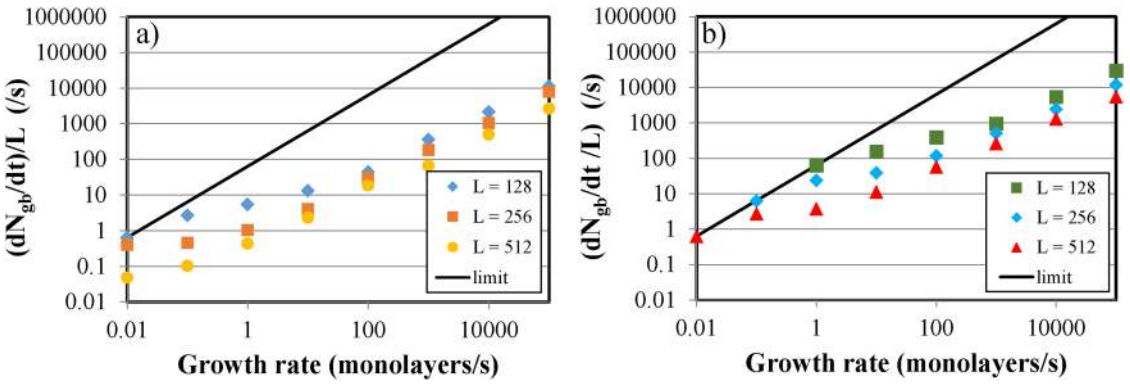

FIG. 6. Rate of atoms jumping into grain boundary normalized by grain size [$(dN_{gb}/dt)/L$] vs growth rate. The film stress has been set to remain at a value of zero so that there are no atoms jumping out of the boundary. Results are shown after 100 monolayers of deposition at simulation temperatures of (a) 300 K and (b) 400 K. The solid line represents the limit of all deposited atoms jumping into the grain boundary.

off the rate of atoms jumping out of the grain boundary (e.g., by setting the X_{gb} simulation parameter to zero). In this case, (dN_{gb}/dt) is equal to $(dN_{gb}/dt)_{in}$. Figure 6 shows the simulation value of $(dN_{gb}/dt)_{in}$ with the stress turned off normalized by grain size for different growth rates and temperature. At high R, the rate exhibits the power-law dependence seen in Fig. 3 for the net flux (dN_{gb}/dt). At lower R, the rate approaches the solid line that corresponds to all the deposited atoms getting to the grain boundary $[(dN_{gb}/dt)_{in}/L \sim R]$.

C. Stress

The simulated steady-state stress has a complex dependence on the growth rate, temperature, and grain size as shown in Fig. 4. For all the temperatures and grain sizes, the stress is tensile at high growth rates and becomes more compressive as the rate is decreased. The transition from tensile to compressive shifts to higher growth rates for smaller grain size and for higher temperatures. Similar to the changes seen in morphology evolution, increasing the growth rate has a similar effect as lowering the diffusivity or temperature.

To understand this behavior, it is useful to look at the quantities that determine the stress, as described by Eq. (2). The time derivative relates the stress evolution to the rate of atoms going into the boundary and the increase in the grain boundary height,

$$\frac{d\sigma}{dt} = \frac{-M_f\, a^3}{L\, h_{gb} w}\left(\frac{dN_{gb}}{dt}\right) + (\sigma_T - \sigma)\frac{\frac{dh_{gb}}{dt}}{h_{gb}}. \tag{4}$$

By setting $(d\sigma/dt)$ equal to zero, we can determine the steady-state stress in the film as

$$\sigma_{SS} = \sigma_T - \frac{M_f a^3}{Lw}\frac{\frac{dN_{gb}}{dt}}{\frac{dh_{gb}}{dt}}. \tag{5}$$

This equation shows that the stress depends on the simulation parameters in several different ways. The tensile stress that is generated when layers in adjacent islands coalesce (σ_T) depends on $(1/L)^{½}$ so it is larger for small grain size. The constant in front of the compressive second term on the right-hand side depends on $1/L$ so it also increases for small grain size. This occurs because insertion of an atom into the grain boundary of a small grain creates more strain than in a large grain. Therefore, the dependence of stress on the grain size also depends on the growth rate. When R is large, the stress is more tensile for small grains than it is for large grains. When R is small, the stress is more compressive for small grains than it is for large grains. This leads to a crossover of the stress vs R curves for different grain sizes that is also seen experimentally.[3]

The kinetics of thin film growth affect the stress through the ratio of the net rate of atoms jumping into and out of the grain boundary (dN_{gb}/dt) to the rate at which the grain boundary height increases (dh_{gb}/dt). The different kinetic regimes can best be seen by inverting Eq. (5) to obtain the ratio

$$\frac{\frac{dN_{gb}}{dt}}{\frac{dh_{gb}}{dt}} = (\sigma_T - \sigma_{SS})\frac{Lw}{M_f a^3}. \tag{6}$$

The dependence of $\frac{dN_{gb}}{dt}/\frac{dh_{gb}}{dt}$ on the growth rate and temperature determined from the steady-state stress is shown in Fig. 7. At large values of R, it has a power-law dependence, reflecting the behavior seen for (dN_{gb}/dt) in Fig. 3. The ratio depends on $R^{(1-x)}$ assuming that dh_{gb}/dt is approximately equal to R. This makes the steady-state stress less tensile when the growth rate is decreased from its largest value.

However, at lower growth rates, the power-law dependence changes to a more constant value that depends on the grain size. This can be understood in terms of the change in the surface morphology evolution. As R decreases, the nucleation rate of new islands on a terrace decreases. This makes it more likely for a

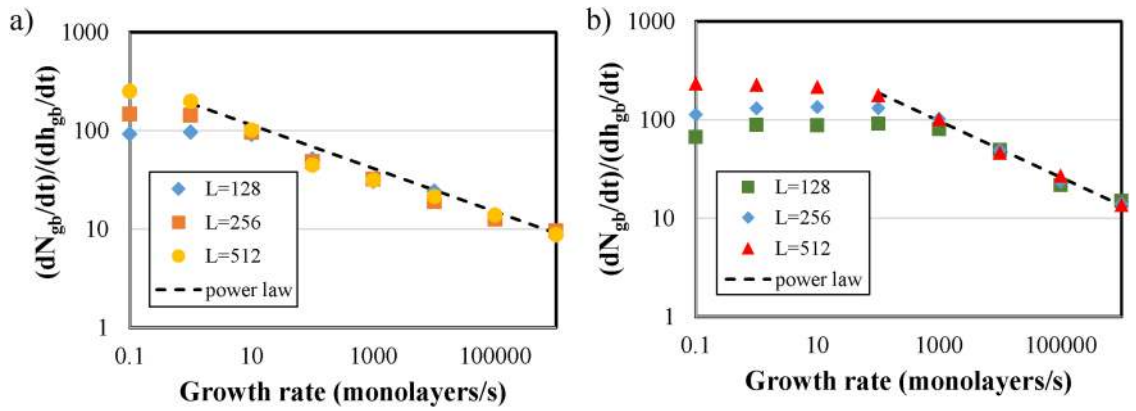

FIG. 7. Net rate of atoms jumping into and out of the grain boundary normalized by the grain boundary growth rate $[(dN_{gb}/dt)/(dh_{gb}/dt)]$ vs growth rate. The ratio is determined from the steady-state stress, as described in the text. Results are shown after 100 monolayers of deposition at simulation temperatures of (a) 300 K and (b) 400 K. The dashed line represents power-law dependence seen at high growth rates.

deposited atom to get to the grain boundary without becoming attached to another adatom or terrace ledge. Atoms going into the grain boundary generate compressive stress, which increases the rate of atoms jumping out of the grain boundary and onto the surface. The net rate ultimately reaches a steady-state and, therefore, the stress also reaches a compressive steady-state. However, the rates of atoms jumping into the grain boundary and out of it have a complex relationship with each other, so the dependence of the stress on the deposition rate cannot be calculated. But it can be seen from the figure that the stress depends less strongly on the growth rate than it does in the power-law regime.

The results in Fig. 7 point to an interesting interplay between the growth kinetics, the grain size, and the stress under different conditions. In the power-law regime (represented by dashed line), the ratio $\frac{dN_{gb}}{dt}/\frac{dh_{gb}}{dt}$ increases as the growth rate decreases indicating that the rate of atoms going into the boundary becomes higher relative to the rate at which the boundary height increases. This tends to make the stress tensile at high growth rates and less tensile as the growth rate is decreased. The power-law exponent does not depend on the grain size, which indicates that the rates depend primarily on what is happening near the grain boundary and not on conditions far away from it. This behavior is observed when the diffusion distance of deposited atoms is small, i.e., at high growth rates or low temperatures. Although the grain size does not affect the rate of transitions at the boundary, it does change the amount of tensile stress generated by island coalescence, σ_T.

When the diffusion distance for deposited adatoms is made larger by lowering the growth rate or raising the temperatures, the surface morphology near the grain boundary is affected by the grain size, as can be seen in Fig. 2. In this case, conditions farther from the boundary affect the step structure and concentration of adatoms at the grain boundary edge. The dependence of the corresponding steady-state stress on the growth rate changes as well, from power-law to a weaker dependence. The stress in this regime is, therefore, more sensitive to the grain size and less dependent on the growth rate.

D. Relaxation and recovery kinetics

The kinetics of relaxation and recovery at $T = 400$ K are shown in Fig. 5 for multiple periods of deposition and relaxation at different grain sizes. The first sequence of growth is performed for 20 monolayers; it is not analyzed since the grain boundary is not well developed in the early stages. After the growth is terminated, the stress is allowed to relax for 32 s. When the growth is resumed, the stress-thickness evolves to a constant slope corresponding to a steady-state stress. The growth is continued for another period of 2 s (20 monolayers) and then followed by another period of relaxation.

To interpret the kinetics of relaxation and recovery, we refer to a kinetic rate equation model that has recently been published[31] that is used to analyze the results of relaxation experiments. The stress-generating mechanisms in the model are the same as those used in the simulation and described by Eq. (2), i.e., tensile stress due to coalescence and compressive stress due to insertion of atoms into the grain boundary. In addition, the grain boundary mobility is assumed to be high so that the stress is uniform throughout the thickness of the film.

The evolution of the stress is based on Eq. (4), but with the appropriate conditions for the case of growth and relaxation. During relaxation, the growth flux is zero so we assume that the grain boundary height does not change ($dh_{gb}/dt = 0$). In addition, the supersaturation on the surface due to the growth flux is assumed to disappear. The evolution of the stress is then described by

$$\frac{d\sigma}{dt} = \frac{-2M_f\, a^2}{L\, h_{gb}} \left[\left(\frac{dN_{gb}}{dt}\right)_{in,0} - \left(\frac{dN_{gb}}{dt}\right)_{out,0} e^{\frac{-(\sigma a^3)}{kT}} \right], \qquad (7)$$

where $(dN_{gb}/dt)_{in,0}$ refers to the rate of atoms jumping into the grain

boundary per surface site at the edge of the boundary when the growth flux is turned off. This cannot be calculated from the simulation parameters because the concentration of atoms in these edge sites is not known. $(dN_{gb}/dt)_{out,0}$ is the analogous rate of atoms jumping out of the boundary at each edge site when there is no additional driving force of stress. This rate can be calculated from the simulation parameters as follows:

$$\left(\frac{dN_{gb}}{dt}\right)_{out,0} = \upsilon X_{gb} e^{\frac{-E_{eff}}{kT}}. \tag{8}$$

As described in Ref. 31, the difference in these rates can be related to the difference in the chemical potential of atoms on the surface relative to the grain boundary ($\Delta\mu_0$),

$$\frac{\left(\frac{dN_{gb}}{dt}\right)_{out,0}}{2\left(\frac{dN_{gb}}{dt}\right)_{in,0}} = e^{\frac{-\Delta\mu_0}{kT}}. \tag{9}$$

In equilibrium, the difference in these rates would lead to a stress in the film. Therefore, $\Delta\mu_0$ can be determined from the final stress that the film relaxes to, i.e., $\sigma_f = \frac{-\Delta\mu_0}{a^3}$.

Equation (7) can be solved to predict the kinetics of the stress relaxation. The time dependent stress is given by

$$\sigma = \sigma_f + \frac{kT}{a^3}\ln\left(1 - \left(1 - e^{\frac{(\sigma_0-\sigma_f)a^3}{kT}}\right)e^{\frac{-\beta D t}{L\,h_{gb}}}\right), \tag{10a}$$

where

$$\frac{\beta D}{L\,h_{gb}} = \frac{-M_f\,a^5}{L\,h_{gb}kT}\left(\upsilon X_{gb} e^{\frac{-E_{eff}}{kT}}\right)e^{\frac{-\sigma_f a^3}{kT}}. \tag{10b}$$

σ_0 is the stress when the relaxation starts, σ_f is the final stress after relaxing for a long time, and βD depends on the kinetics.

The unknown parameters in this equation $\left(\sigma_f \text{ and } \frac{\beta D}{L\,h_{gb}} \equiv \frac{1}{\tau}\right)$ are determined by fitting the relaxation data to this form. The results of the fitting are shown as the solid lines in Fig. 5 and show that the model can capture the kinetics of relaxation. The corresponding values of the fitting parameters are given in Table II.

TABLE II. Parameters σ_f and $\frac{1}{\tau}$ obtained from fitting the stress relaxation data shown in Fig. 5. Final column is value of $\frac{\beta D}{L\,h_{gb}}$ calculated from the simulation parameters for comparison with the fitting parameter $\frac{1}{\tau}$.

Grain size (L)	Thickness (monolayers)	σ_f (GPa)	$\frac{1}{\tau}(1/s)$	$\frac{\beta D}{L\,h_{gb}}(1/s)$ calculated from simulation parameters
128	20	−0.1772	0.2328	12.733 190 8
128	40	−0.1643	0.226	5.976 192 161
256	20	−0.2096	0.2846	7.463 345 754
256	40	−0.224	0.2436	4.004 810 087
512	20	−0.1894	0.0581	3.379 626 011
512	40	0.9673	0.000 160 7	0.005 801 72

To describe the kinetics of recovery, the stress evolution can be calculated using the conditions present during deposition,

$$\frac{d\sigma}{dt} = \frac{-2M_f\,a^2}{L\,h_{gb}}\left(\frac{dN_{gb}}{dt}\right)_{in,0}\left[e^{\frac{\delta\mu_s}{kT}} - e^{\frac{-(\sigma a^3+\Delta\mu_0)}{kT}}\right] + (\sigma_T - \sigma)\frac{\frac{dh_{gb}}{dt}}{h_{gb}}. \tag{11}$$

$\delta\mu_s$ describes the increase in chemical potential of atoms on the surface when a growth flux is present. Assuming that the grain boundary height is approximately the same as the film thickness, then $\frac{\frac{dh_{gb}}{dt}}{h_{gb}} \sim \frac{R}{h_0+Rt}$, where t is the time after the film growth is resumed and .. is the thickness when the growth is resumed.

This equation can be solved if the exponential terms are approximated by linearizing them,

$$\frac{d\sigma}{dt} = \frac{-2M_f\,a^2}{L\,h_{gb}}\left(\frac{dN_{gb}}{dt}\right)_{in,0}\frac{\delta\mu_s + \sigma a^3 + \Delta\mu_0}{kT} + (\sigma_T - \sigma)\frac{R}{h_0 + Rt}. \tag{12}$$

The stress has the form

$$\sigma = \sigma_{ss} + \frac{\sigma_0 - \sigma_{ss}}{\left(1 + \frac{Rt}{h_0}\right)^A}, \tag{13}$$

where the exponent A is equal to $\left(1 + \frac{\beta D}{RL}\right)$. σ_o is the stress when the growth is resumed at $t = 0$ and σ_{SS} is the steady-state stress during growth at rate R. The unknown parameters (σ_{SS} and A) are determined by fitting the recovery kinetics to this form. The calculated values from the fitting are shown as the solid lines in the figure. The corresponding parameters are listed in Table III.

The kinetic parameter βD plays a role in both the relaxation and the recovery. Since βD is not expected to depend strongly on the grain size, the relaxation rate $\left(\frac{1}{\tau}\right)$, which is equal to $\frac{\beta D}{L\,h_{gb}}$, should depend inversely on the grain size and grain boundary height. Figure 8(a) presents a plot of $\frac{1}{\tau}$ obtained from the fitting vs $\frac{1}{L\,h_{gb}}$, which shows such a trend. For comparison, the value of $\frac{\beta D}{L\,h_{gb}}$ can also be calculated from the simulation parameters using Eq. (10b).

TABLE III. Parameters σ_{SS} and A obtained from fitting the stress recovery data shown in Fig. 5. Final column is value of $1 + \frac{\beta D}{RL}$ estimated from the simulation parameters for comparison with the fitting parameter A.

Grain size (L)	Starting thickness (monolayers)	σ_{SS} (GPa)	A	$1 + \frac{\beta D}{RL}$ calculated from simulation parameters
128	20	−1.1498	50.33	26.466 381 6
256	20	−1.097	43.98	15.926 691 51
512	20	−1.105	24.809	7.759 252 023

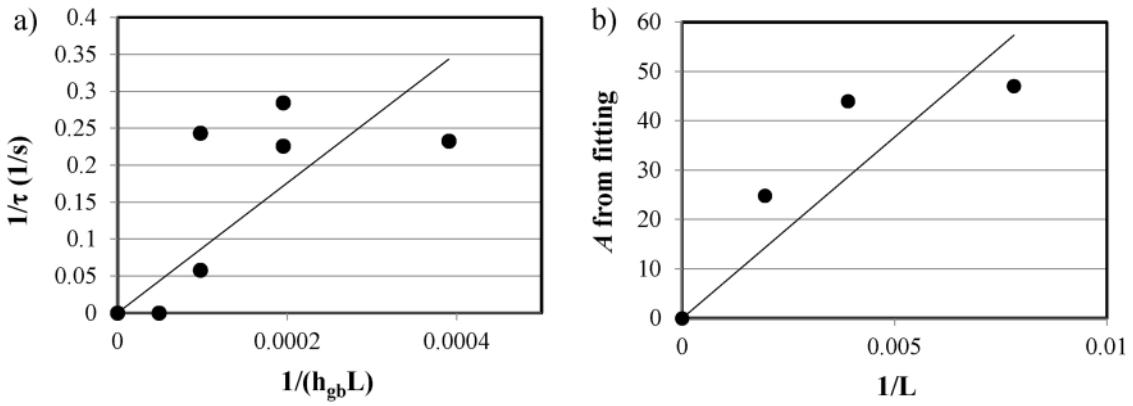

FIG. 8. (a) Parameter obtained from fitting relaxation kinetics $\left(\frac{1}{\tau}\right)$ vs $1/h_{gb}L$. (b) Parameter obtained from fitting stress recovery (A) vs $1/L$.

The calculated values (shown in the final column of Table II) are consistently higher than those obtained from fitting by more than an order of magnitude. This discrepancy may be related to a difference between the assumptions used for calculating the relaxation kinetics and what occurs in the simulation. The calculations assume that the deposition-induced change in chemical potential ($\delta\mu_s$) goes to zero during relaxation so that the number of atoms jumping into the grain boundary should be low. However, the simulation shows that the rate of atoms jumping into the boundary remains similar to the rate of atoms coming out of it. We believe this is because of the relatively flat surface morphology, which means that atoms that come out of the grain boundary cannot find sinks on the surface and, therefore, are likely to jump back into the grain boundary. This makes the net rate (i.e., the difference between rates into and out of the grain boundary) much smaller than predicted by the model in Eq. (7), consistent with what is seen in the relaxation simulations. The relaxation kinetics still seem to agree with the form described by Eq. (10), which may be because the rates in and out remain roughly proportional to each other during relaxation. The implication for stress evolution in real films is that the kinetics of relaxation are more complicated than simply diffusion out of the grain boundary and depend on the details of the transition region between the grain boundary and the surface.

Similarly, the parameter for recovery A, which is equal to $\left(1+\frac{\beta D}{RL}\right)$, should depend linearly on $1/L$. The plot of A vs $1/L$ [Fig. 8(b)] shows a roughly linear dependence. The value of $1+\frac{\beta D}{RL}$ can also be calculated from the simulation parameters for comparison with the results obtained from fitting the recovery data (shown in final column of Table III). The agreement between the calculated value and the fitting is much closer than for relaxation and the values only differ by a factor of 2–3. This suggests that the conditions during recovery are more similar to the assumptions of the calculation than relaxation.

V. CONCLUSIONS

The KMC simulations enable us to see the processes that control stress evolution in thin films. They illustrate the interrelationship between the surface morphology, the rate of transitions into and out of the grain boundary, and the resulting stress. When the diffusion distance of a deposited atom is small (high R, low T), the rate of cluster nucleation is high and the morphology is relatively uniform across the surface. Therefore, the rate of jumping into the grain boundary does not depend on the grain size and the dependence of the stress is primarily due to the change in tensile stress from coalescence. Increasing the diffusion distance (lower R, higher T) causes a transition to growth controlled by the flow of steps. As atoms diffuse larger distances, the surface concentration at the grain boundary edge is affected by conditions further away. Hence, the grain boundary transition rates and the resulting stress become more dependent on the grain size.

The relaxation and recovery kinetics also depend on the grain size. Although the form of the relaxation kinetics is in agreement with the predictions of an analytical model, the rate of relaxation is much slower than expected from the simulation parameters. This may be due to a deviation from the assumption that the surface supersaturation disappears when the growth flux is terminated. It also reveals that the evolution of the surface morphology near the grain boundary during relaxation may be complicated by the addition of atoms coming from the grain boundary. The kinetics of recovery when growth is resumed agree more closely with the predictions of the analytical model.

The simulation programs developed in this work are not currently available for use by others. However, we would be glad to work with researchers who are interested in KMC modeling of stress evolution during thin film growth.

ACKNOWLEDGMENTS

This work was supported by the National Science Foundation (NSF) under Contract Nos. DMR-1602491 and DMR-2006422.

DATA AVAILABILITY

The data that support the findings of this study are available from the corresponding author upon reasonable request.

REFERENCES

[1]S. J. Hearne and J. A. Floro, J. Appl. Phys. **97**(1), 014901 (2005).
[2]H. Z. Yu and C. V. Thompson, Acta Mater. **67**, 189 (2014).
[3]A. M. Engwall, Z. Rao, and E. Chason, Mater. Des. **110**, 616 (2016).
[4]D. Chocyk, T. Zientarski, A. Proszynski, T. Pienkos, L. Gladyszewski, and G. Gladyszewski, Cryst. Res. Technol. **40**(4–5), 509 (2005).
[5]R. Abermann, Vacuum **41**(4–6), 1279 (1990).
[6]G. Thurner and R. Abermann, Thin Solid Films **192**(2), 277 (1990).
[7]R. Koch, D. Hu, and A. K. Das, Phys. Rev. Lett. **94**(14), 146101 (2005).
[8]D. Winau, R. Koch, A. Fuhrmann, and K. H. Rieder, J. Appl. Phys. **70**(6), 3081 (1991).
[9]H. J. Schneeweiss and R. Abermann, Vacuum **43**(5–7), 463 (1992).
[10]E. Chason, J. W. Shin, S. J. Hearne, and L. B. Freund, J. Appl. Phys. **111**(8), 083520 (2012).
[11]S. C. Seel, C. V. Thompson, S. J. Hearne, and J. A. Floro, J. Appl. Phys. **88**(12), 7079 (2000).
[12]Z. Rao, S. J. Hearne, and E. Chason, J. Electrochem. Soc. **166**(1), D3212 (2019).
[13]D. Flötotto, Z. M. Wang, L. P. H. Jeurgens, and E. J. Mittemeijer, J. Appl. Phys. **118**(5), 055305 (2015).
[14]M. F. Doerner and W. D. Nix, Crit. Rev. Solid State Mater. Sci. **14**(3), 225 (1988).
[15]R. Koch, J. Phys. Condens. Matter **6**(45), 9519 (1994).
[16]E. Chason and P. R. Guduru, J. Appl. Phys. **119**(19), 191101 (2016).
[17]G. Abadias, E. Chason, J. Keckes, M. Sebastiani, G. B. Thompson, E. Barthel, G. L. Doll, C. E. Murray, C. H. Stoessel, and L. Martinu, J. Vac. Sci. Technol. A **36**(2), 020801 (2018).
[18]R. W. Hoffman, Thin Solid Films **34**(2), 185 (1976).
[19]W. D. Nix and B. M. Clemens, J. Mater. Res. **14**(8), 3467 (1999).
[20]L. B. Freund and E. Chason, J. Appl. Phys. **89**(9), 4866 (2001).
[21]E. Chason, B. W. Sheldon, L. B. Freund, J. A. Floro, and S. J. Hearne, Phys. Rev. Lett. **88**(15), 156103 (2002).
[22]A. M. Engwall, Z. Rao, and E. Chason, J. Electrochem. Soc. **164**(13), D828 (2017).
[23]E. Chason, A. M. Engwall, Z. Rao, and T. Nishimura, J. Appl. Phys. **123**(18), 185305 (2018).
[24]E. Chason, M. Karlson, J. J. Colin, D. Magnfalt, K. Sarakinos, and G. Abadias, J. Appl. Phys. **119**(14), 145307 (2016).
[25]T. Kaub, Z. X. Rao, E. Chason, and G. B. Thompson, Surf. Coat. Technol. **357**, 939 (2019).
[26]J. W. Evans, P. A. Thiel, and M. C. Bartelt, Surf. Sci. Rep. **61**(1–2), 1 (2006).
[27]H. Huang, G. H. Gilmer, and T. Díaz de la Rubia, J. Appl. Phys. **84**(7), 3636 (1998).
[28]G. H. Gilmer, H. C. Huang, T. D. de la Rubia, J. Dalla Torre, and F. Baumann, Thin Solid Films **365**(2), 189 (2000).
[29]H. N. G. Wadley, A. X. Zhou, R. A. Johnson, and M. Neurock, Prog. Mater. Sci. **46**(3–4), 329 (2001).
[30]E. Chason and A. F. Bower, J. Appl. Phys. **125**(11), 115304 (2019).
[31]P. Jagtap and E. Chason, Acta Mater. **193**, 202 (2020).
[32]E. Chason and B. W. Dodson, J. Vac. Sci. Technol. A **9**(3), 1545 (1991).
[33]E. Chason, W. L. Chan, and M. S. Bharathi, Phys. Rev. B **74**(22), 224103 (2006).
[34]M. J. Rost, Phys. Rev. Lett. **99**(26), 266101 (2007).